frontiers in Earth Science

ORIGINAL RESEARCH
published: 19 June 2020
doi: 10.3389/feart.2020.00200

Surface Ocean Hydrographic Changes in the Western Pacific Marginal Seas Since the Early Holocene

Hui-Juan Pan[1], Min-Te Chen[1,2,3]*, Deming Kong[4], Xiaopei Lin[5], Kuo-Tsan Wong[6], Hung-Ling Tsai[1], Shengfa Liu[7,8], Xuefa Shi[7,8] and Yosuke Yokoyama[9]*

[1] Institute of Earth Sciences, College of Ocean Science and Resource, National Taiwan Ocean University, Keelung, Taiwan, [2] Center of Excellence for Ocean Engineering, College of Engineering, National Taiwan Ocean University, Keelung, Taiwan, [3] Center of Excellence for Oceans, National Taiwan Ocean University, Keelung, Taiwan, [4] Laboratory for Coastal Ocean Variation and Disaster Prediction, College of Ocean and Meteorology, Guangdong Ocean University, Zhanjiang, China, [5] Key Laboratory of Physical Oceanography, College of Ocean and Atmospheric Science, Ocean University of China, Qingdao, China, [6] Central Geological Survey, Ministry of Economic Affairs, New Taipei City, Taiwan, [7] Key Laboratory of Marine Sedimentology and Environmental Geology, First Institute of Oceanography, State Oceanic Administration, Qingdao, China, [8] Laboratory for Marine Geology, Qingdao National Laboratory for Marine Science and Technology, Qingdao, China, [9] Atmosphere and Ocean Research Institute, The University of Tokyo, Kashiwa, Japan

OPEN ACCESS

Edited by:
Hai Xu,
Tianjin University, China

Reviewed by:
Xin Zhou,
University of Science and Technology of China, China
Xianyu Huang,
China University of Geosciences Wuhan, China

***Correspondence:**
Hui-Juan Pan
hjpan76@gmail.com
Min-Te Chen
mtchen@mail.ntou.edu.tw

Specialty section:
This article was submitted to Quaternary Science, Geomorphology and Paleoenvironment, a section of the journal Frontiers in Earth Science

Received: *03 March 2020*
Accepted: *18 May 2020*
Published: *19 June 2020*

Citation:
Pan H-J, Chen M-T, Kong D, Lin X, Wong K-T, Tsai H-L, Liu S, Shi X and Yokoyama Y (2020) Surface Ocean Hydrographic Changes in the Western Pacific Marginal Seas Since the Early Holocene. Front. Earth Sci. 8:200. doi: 10.3389/feart.2020.00200

Climatic changes in the western Pacific marginal seas are influenced by global forcing and regional processes, including monsoons, and ocean circulation. To better understand the process of hydrographic and temperature changes, we applied the $U^{K'}_{37}$ as our index of Sea Surface Temperature (SST) and TEX_{86} as the index of Subsurface Water Temperature (SWT) for the last 8400 years using the sediment core MZ01 from the continental shelf of the East China Sea (ECS). To focus on centennial and millennial variabilities, the original SST and SWT are filtered with the Ensemble Empirical Mode Decomposition (EEMD) of the Hilbert-Huang Transform (HHT), with the confidence defined by a new method, the Continuity Superposition Error Calculation Method (CSECM). The SST and SWT both have a quasi-period of 1000–2000 years, exhibiting some teleconnection with the north Atlantic climatic changes. The SWT decreased during approximately 6–4 ka and then increased by ∼4°C to the late Holocene, almost anti-phase with the SST. The stronger Asian winter monsoon and China Coastal Current (CCC), are very likely responsible for the decreased SST in the late Holocene. In contrast, the increased SWT may imply that the stronger CCC has brought more Changjiang Diluted Water (CDW) southward and formed a thicker barrier layer in the ECS, which dampened bottom water heat loss that was transported from the Taiwan Warm Current (TWC), and Western Kuroshio Branch Current (WKBC). This process is tested by the hosing experiment that supports stronger stratification when the north Atlantic cooled. The combined results by $U^{K'}_{37}$ and TEX_{86} provide a new insight into the interaction mechanism among the winter monsoon, precipitation and the Kuroshio Current, and also raises caution to take more regional factors into account in the application of TEX_{86}.

Keywords: East China Sea, $U^{K'}_{37}$, TEX_{86}, Sea Surface Temperature, East Asia Monsoon, Kuroshio, Hilbert Huang Transform, Ensemble Empirical Mode Decomposition

INTRODUCTION

In past decades, sea surface temperature (SST) reconstructions have depicted quite a consistent portrait of Holocene climatic changes over the open oceans (Leduc et al., 2010; PAGES Ocean 2k Working Group, 2012). In contrast, climatic records from marginal seas always show high complexity and discordance among different regions. This is partly due to the complex effect of terrestrial process, regional currents, and tidal and depositional processes on the marginal seas. In other words, the paleoceanographic records in marginal seas usually contain more climatic information than the open oceans. It is sometimes important to decipher the complex interaction between different forcing, particularly land-ocean interaction. In addition, marginal sea sediments usually provide a higher depositional rate and temporal resolution, which is crucial to reconstruct and understand high resolution climatic changes on centennial to millennial scales.

Previous reconstructions in the western Pacific marginal seas, including the East China Sea (ESC), South China Sea (SCS), and Yellow Sea, show significant influence from the continental climatic system, such as the winter monsoon. Initial comparison between the Holocene SST trend from marginal sea (Kong et al., 2014) and the North Atlantic (Sachs, 2007; Rodrigues et al., 2009) exhibit good agreement in the cooling trend during the mid-late Holocene. This implies possible teleconnection between high latitudes of the North Atlantic Ocean and Pacific marginal seas. The Holocene climate in the North Atlantic has been found to have ∼1500 years quasi-periodic cycles (Bond et al., 1997; Bond et al., 2001). However, little is known about these quasi-periodic cycles in the western Pacific marginal seas (Jian et al., 2000; Kubota et al., 2010; Yi et al., 2015), partly due to the lack of studies and an effective method to extract periodic signals from complicated reconstructions.

Here we report paired temperature reconstruction based on long-chain alkenones and Glycerol Dialkyl Glycerol Tetraethers (GDGTs) over the last 8400 years, and introduce a Continuity Superposition Error Calculation Method (CSECM) to assess the errors in both ages and proxies. We focus on the general trend of surface and subsurface temperature at millennial scales, and attempt to investigate the hydrographic changes in the Western Pacific marginal seas since the early Holocene.

MATERIALS AND METHODS

Sediment Core

The study is based on the continental shelf mud area of the ECS. A sediment core MZ01 (120°50.94′E, 26°32.82′N) was collected from the ECS inner shelf (Liu et al., 2010). The core site is about 65 m in depth and 90 km from the mouth of the Min River, which has a catchment area of approximately 6×10^4 km^2. About 500 km to the north of the core site is the mouth of China's largest river, the Yangtze River (Changjiang; **Figure 1**). The climate system and the hydrological regime prevailing in the study area are demonstrated in the **Supplementary Material**.

The core MZ01 was 2.96 m in total, and it was subsampled at 2 cm intervals and analyzed for grain size, major elements, and clay minerals with five old age dating (Liu et al., 2010). In this study we presented a new age model of core MZ01 that was based on new 12 AMS ^{14}C ages using strictly-selected, mixtures of benthic foraminifers (mainly epifauna; **Supplementary Table S1**). All the calibration and establishment of age are discussed in the **Supplementary Material**.

Analysis of Alkenones and GDGTs

The analyses for long-chain alkenones and GDGTs were performed at the National Taiwan Ocean University using the procedures described by Hung (2013), Tsai (2013), and Lin et al. (2014). The SST was calculated using the empirical equation established by Conte et al. (2006):

$$\mathrm{SST} = -0.957 + 54.293\left(\mathrm{U}^{\mathrm{K}'}_{37}\right) - 52.894\left(\mathrm{U}^{\mathrm{K}'}_{37}\right)^2 + 28.321\left(\mathrm{U}^{\mathrm{K}'}_{37}\right)^3$$

The TEX_{86} was calculated to temperature in the BAYSPAR (BAYesian SPAtially-varying Regression) system[1] (Tierney and Tingley, 2014, 2015), which allows us to predict the temperature empirically derived from regional environmental and biological factors. The uncertainties originating from the BAYSPAR calibration is about ±2.5°C. The BIT (Branched and Isoprenoid Tetraether) index that reflects the terrestrial contribution were established by Hung (2013) and shown in **Supplementary Figure S3**.

Data Processing

Uncertainties in the age controls (X) and proxy data (Y) are always inevitable in paleoclimatic reconstructions. The commonly used methods to assess the uncertainties of a paleoclimatic record include plotting error bars on the X or Y axis, or just describing them in words. However, these methods usually fail to take into account the interrelationship between the errors in X and Y. In an effort to overcome such problems, we introduce the method named CSECM that combines the errors in both X and Y. The CSECM method generally includes four steps, which are elaborated in the **Supplementary Material**.

The Hosing Experiment

To test the impact of global climatic forcing such as the change of AMOC (Atlantic Meridional Ocean Circulation; van Oldenborgh et al., 2009; Svendsen et al., 2014) to the surface hydrographies in the western Pacific marginal seas, we used data from the run the National Center for Atmospheric Research (NCAR) Community Climate System Model version 3 (CCSM3). The CCSM3 is a fully coupled model, comprised of the Parallel Ocean Program (POP), the Community Atmosphere Model (CAM), the Community Sea Ice Model (CSIM), and the Community Land Model (CLM). The resolution configuration of the model is referred to as T42 × 1. CAM uses spectral dynamics at T42 resolution (grid spacing of approximately 2.8° in latitude and longitude with 26 vertical

[1]https://github.com/jesstierney/BAYSPAR

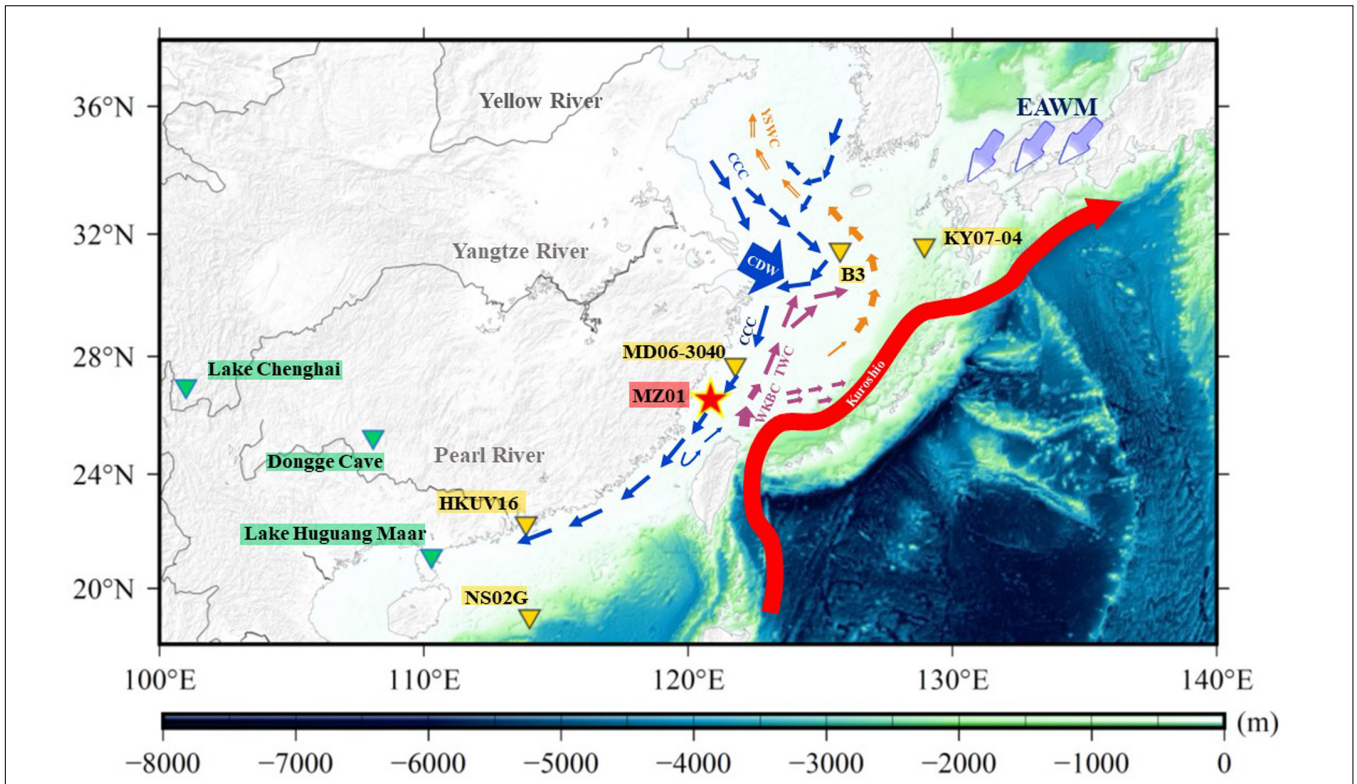

FIGURE 1 | Topography of the study area close to site MZ01 (red star) and the fluvial systems on surrounding continents. Also shown are locations of oceanic archive KY07-04 (Nakanishi et al., 2012), B3 (Zhao et al., 2014), MD063040 (Wang et al., 2014), HKUV16 (Kong et al., 2014), NS02G (Kong et al., 2014) labeled with yellow triangles; and terrestrial archives Dongge Cave (Dykoski et al., 2005), Lake Huguang Maar (Yancheva et al., 2007), and Lake Chenghai (Xu et al., 2020) labeled with green triangles. The arrows show monsoon winds and current systems: Kuroshio Current, Western Kuroshio Branch Current (WKBC), Taiwan Warm Current (TWC), and Changjiang Diluted Water (CDW) after Lie and Cho (2016); Chinese Coastal Current (CCC) after Lee and Chao (2003); and Yellow Sea Warm Current (YSWC) after Bian et al. (2013).

hybrid levels). The ocean grid has 320 × 384 horizontal points, with enhanced meridional resolution near the equator and high-latitude North Atlantic, and 40 levels in the vertical z-coordinate. The ice model shares the same horizontal resolution with the ocean model. The North Pole is set in Greenland to avoid singularity problems.

The control setting is Holocene climatological means, which is represented using the mean condition of the last 30 years. The experimental setting is the shut-down status of AMOC caused by 1 Sv (Sverdrup) fresh water impulses during the Bond or Heinrich-type cold events (Stouffer et al., 2006). The fresh water hosing lasts for 100-years, which is sufficient to shut down the AMOC, and the experiments are termed hosing experiments. Based on the hosing experiment results, parameter differences between experimental and control settings were plotted, respectively, for winter and summer (**Figure 2**).

RESULTS

According to the age model, the core MZ01 extends back to 8400 years BP, with an average sedimentation rate ∼33.6 cm/kyr. The sedimentation rate was much higher during the period 8.5–7.5, 6–5, and 1–0 ka (**Supplementary Figure S2**). As a result, the resolution of the reconstructed record varied greatly at different stages, possibly due to dynamic sedimentation processes in the shelves of the ECS (Yang et al., 2016; Liu et al., 2018).

The $U^{K'}_{37}$-SST of MZ01 ranges within 23.2–26.8°C and can be roughly divided into 3 stages: fast fluctuation from 8.4 to 6 ka, warming from ∼6 to 3 ka, and mild cooling since 3 ka (**Figure 3**). The record is imbedded with several fast cooling events at ∼7.6, ∼6.1, ∼5.5, and ∼1.0 ka. In the past 1 ky, relatively warmer and cooler periods could be identified, within the ranges of age and proxy uncertainties, at approximately 0.8–0.4 and 0.4–0.1 ky BP. Despite the age uncertainties and small temperature differences between these two periods, they might be hydrographic fingerprints from the widely found "Medieval Warm Period" and "Little Ice Age."

The TEX_{86}-derived temperature calculated by the BAYSPAR system range from 14.5–24.7°C (**Figure 3**), about 2°C lower than the result obtained from calibration by Kim et al. (2010). The core top TEX_{86}-Subsurface Water Temperature (SWT) is about 17.4°C, lower than the observed subsurface seawater temperature (21°C) near the core site. Generally, the TEX_{86}-derived temperature shows quite different changes from the $U^{K'}_{37}$-SST. It fluctuated greatly and decreased from 8.4 ka to

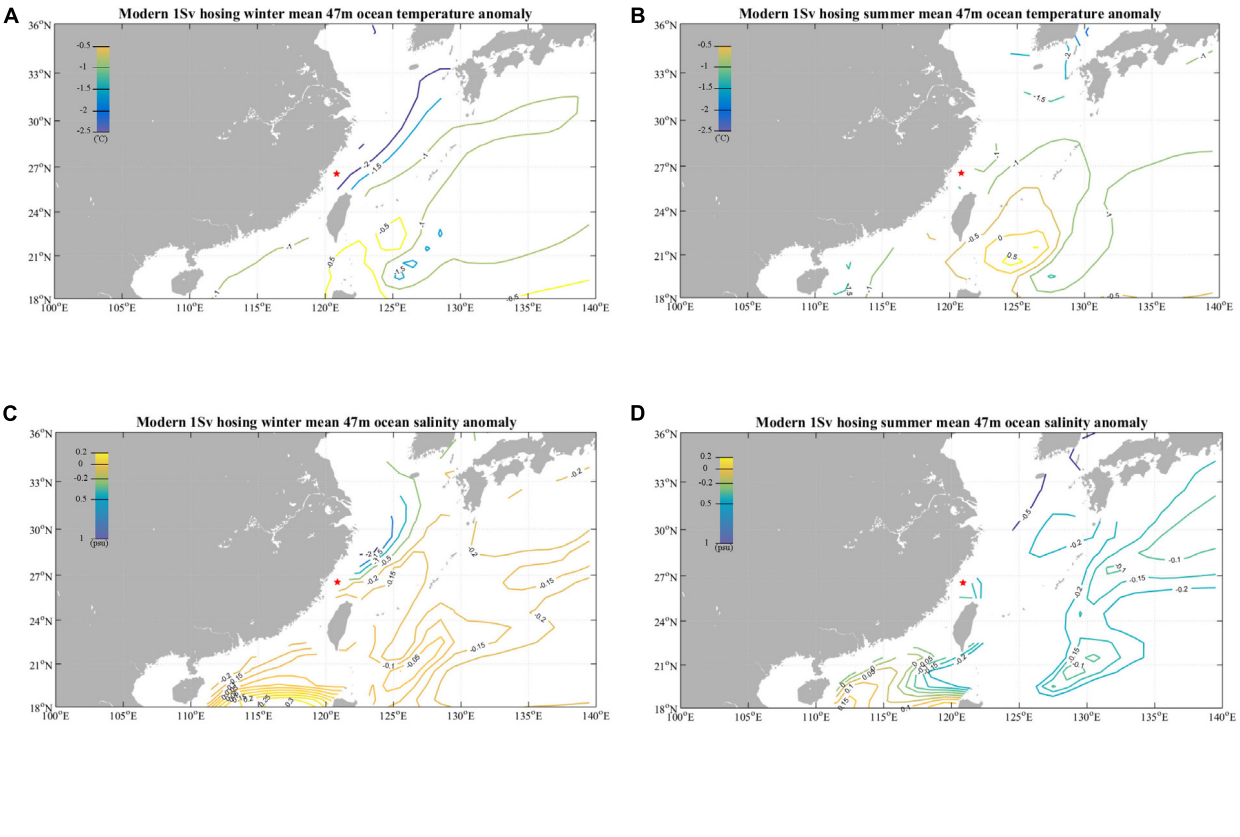

FIGURE 2 | Spatial distribution of temperature **(A,B)** and salinity **(C,D)** in winter **(A,C)** and summer **(B,D)**. Contours reveal the status at a depth of 47 m during AMOC shut-down according to the hosting experiments.

~6.6 ka. After a cold period between 7–6 ka, the temperature rapidly increased to the episodic maximum at 6 ka, and decreased to ~4 ka. It then exhibits an apparently increasing trend with two coolings at 2.4 ka and 1.0ka.

As the original $U^{K'}_{37}$-SST and TEX_{86}-SWT contain some noise signal and errors in both age and proxy data, we prefer to discuss the trend of these two proxies. The trend of $U^{K'}_{37}$-SST and TEX_{86}-SWT were named the $U^{K'}_{37}$-SST-trend2 ($=\sum_{i=2}^{n} IMFi + R$), and TEX_{86}-SWT-trend2 ($=\sum_{i=2}^{n} IMFi + R$). The trend lines were plotted with the error range provided by the CSECM (**Figure 3**).

The TEX_{86}-SWT of MZ01 shows several warming-cooling cycles, with episodic peaks at 7.1, 6.0, 2.8, 1.7, and 0.4 ka. The Hilbert-Huang Transform (HHT) spectrum exhibits cyclicity of approximately 1000–2000 years over the last 8000 years (**Figure 4**).

DISCUSSION

Interpretation of the $U^{K'}_{37}$ and TEX_{86} Proxies

The proxy $U^{K'}_{37}$ has been widely accepted as a good indicator for SST. In this study, the estimated SST from core top (2-points average) $U^{K'}_{37}$ of MZ01 is 26°C, ~4.4°C higher than the observed annual mean SST (21.6°C). The offset between this estimated $U^{K'}_{37}$-SST and the observed SST was also reported in the Pearl River Estuary (Kong et al., 2014). This systematic offset might relate to the different species fraction of coccolithphores (Kang et al., 2016), as well as the different seasonality of alkenone production in various environmental settings (Popp et al., 2006). However, we prefer to consider that the offset between the estimated $U^{K'}_{37}$-SST and "actual" SST had not changed much as long as the environment was relatively stable during the investigated period. In addition, we focus on the general trend rather than details. Thus, the $U^{K'}_{37}$ is expected to be able to reflect the general SST changes in the study area.

The TEX_{86} derived temperature of core top (2-points average) is 21°C, quite close to the annual mean temperature of the whole water column. Analysis of GDGTs in suspended particulate matter suggest that TEX_{86} correlates well with annual mean temperature when the water depth exceeds 70 m in the ECS (Zhang et al., 2017). While sediment TEX_{86} usually shows a much lower estimated value than the observed temperature in the inner shelf (Wei et al., 2011; Zhang et al., 2013). The TEX_{86} was proposed to reflect SWT (Huguet et al., 2006; Jia et al., 2012) and has been adopted by many studies (Li et al., 2013). With the best interpretation on the TEX_{86} proxy,

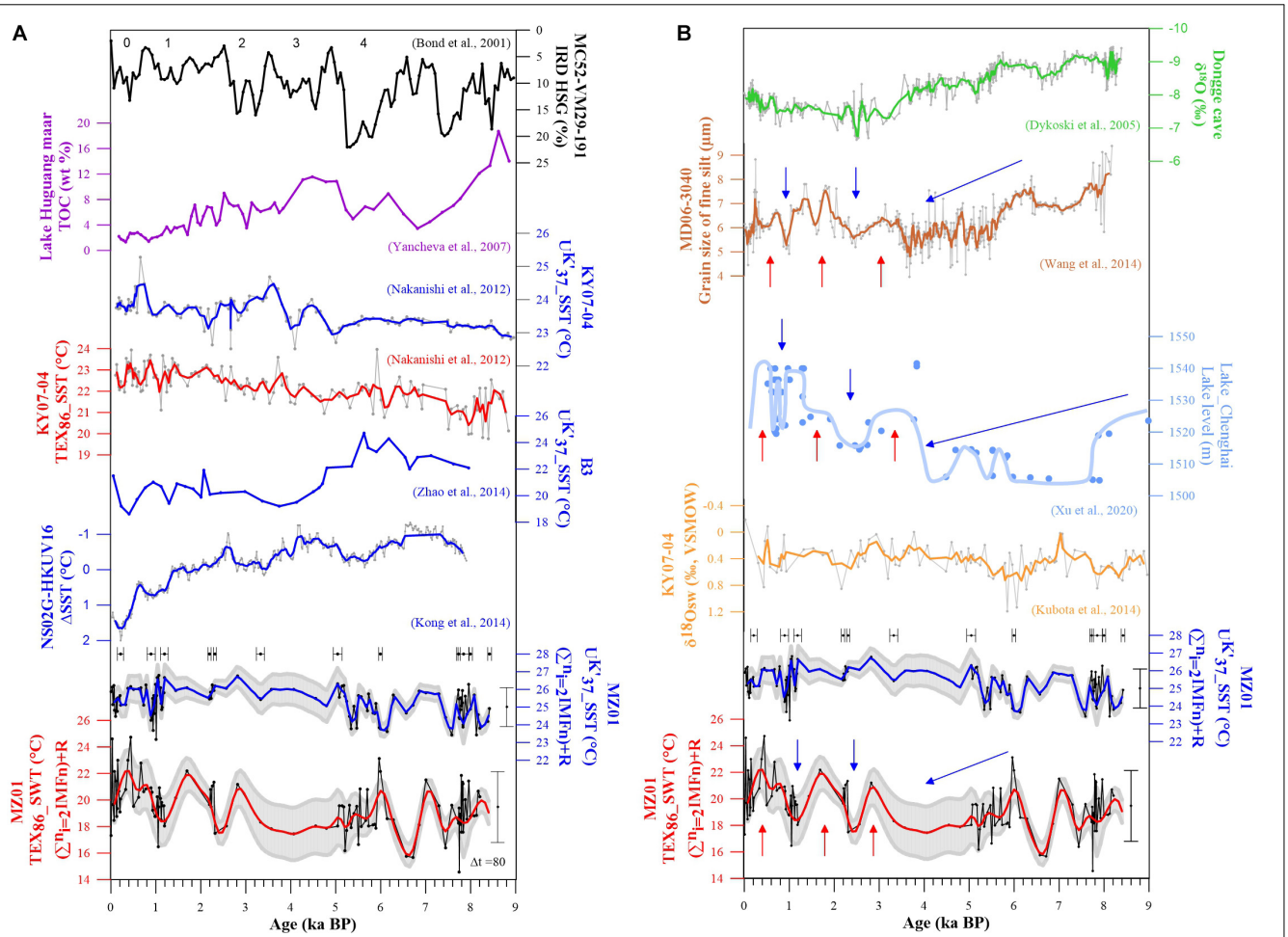

FIGURE 3 | (A) from top to bottom: the variations of hematite-stained grains derived from ice-rafted debris in the North Atlantic (Bond et al., 2001), total organic carbon content in Lake Huguang Maar (Yancheva et al., 2007), $U^{K'}_{37}$-SST and TEX_{86} -derived temperature of core KY07-04 in East China Sea (ECS; Nakanishi et al., 2012), $U^{K'}_{37}$-SST of core B3 in the continental shelf of the ECS (Zhao et al., 2014), and the temperature difference between sites HKUV16 and NS02G neighboring Pearl River estuary (Kong et al., 2014). **(B)** from top to bottom: the fluctuations of $\delta^{18}O$ in Dongge Cave (Dykoski et al., 2005), fine silt grain size of core MD06-3040 from mud belt off the Zhejiang-Fujian coast on the inner shelf of ECS (Wang et al., 2014), lake level variation of Chenghai (Xu et al., 2020), and $\delta^{18}O$ of core KY07-04 (Kubota et al., 2015). The gray curves represent the original data before 3-points smoothing. The last two curves in both **(A)** and **(B)** display the $U^{K'}_{37}$ and TEX_{86} -derived temperature of core MZ01. The gray strip region indicates the temperature range generated from CSECM conversion (**Supplementary Material Part 3**).

it was assumed to record changes in the SWT during our investigational period.

Regional SST and SWT in the ECS Since the Early Holocene

Regional circulations have a strong influence on the temperature and salinity distribution in the ECS. It has been suggested that the modern circulation pattern had not been established until approximately 7–6 ka when the sea level rose to almost modern height (Li et al., 2009; Yuan et al., 2018). The $U^{K'}_{37}$-SST and TEX_{86}-SWT of MZ01 both experienced a cooling between 7–6 ka, implying an impact of the circulation changes on these two proxies. However, it might not be so convincing to give too much weight to the interpretation of temperature changes before 6 ka based on the knowledge of modern circulation.

The $U^{K'}_{37}$-SST of MZ01 increased by ∼2°C from approximately 6 to 3 ka; this seems to coincide with the warming in $U^{K'}_{37}$-SST of the northeastern ECS (site KY07-04) from 6 to 3.5 ka (Nakanishi et al., 2012). Both circumstances may arise from the weakened EAWM that not only caused the warming at site KY0704 but also diminished the cold freshwater supply from China Coastal Current (CCC) to the MZ01. Nevertheless, another $U^{K'}_{37}$-SST (core B3) in the northern ECS shows extraordinary cooling by ∼4°C during this period (Zhao et al., 2014). It was proposed that such cooling anomaly likely relates to the southward migration of the Intertropical Convergence Zone (ITCZ), Western Pacific Subtropical High moving north-westward and strengthening of the Yellow Sea Coastal Current inducing the cold eddy formation (Zhao et al., 2014; Yuan et al., 2018; Xu et al., 2020).

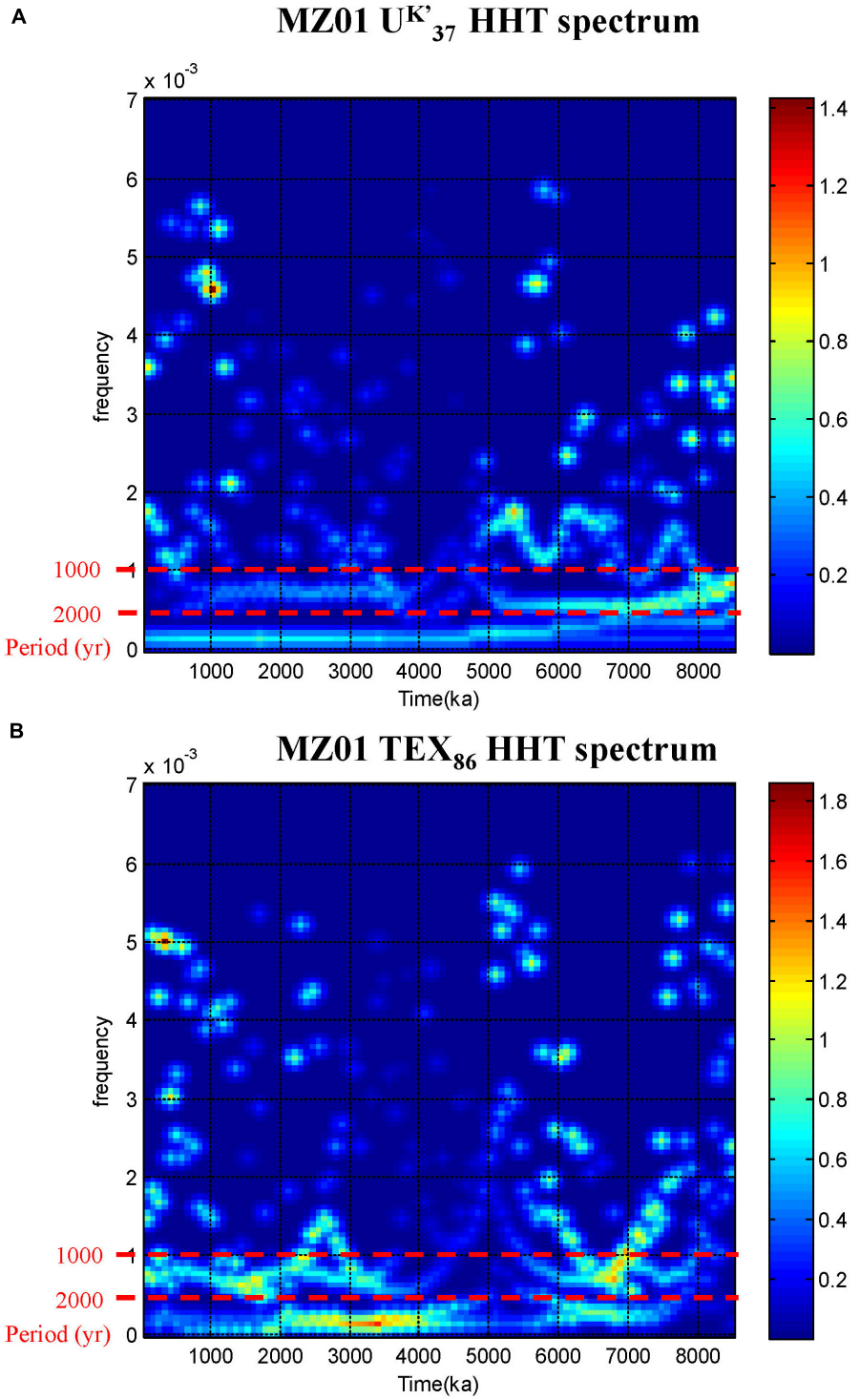

FIGURE 4 | HHT spectrum of MZ01 $U^{K'}_{37}$ SST **(A)** and TEX_{86} -derived temperature **(B)**. The colors between the periodicities of 1000 to 2000 year shown by dash lines indicate the spectral power. We note that the interpretation on spectral power of <1000–2000 year between ~5–2.5 ka is uncertain due to very low sedimentation rate of core MZ01.

On the other hand, the TEX_{86} -derived temperature of core KY07-04 show an overall warming through the Holocene (Nakanishi et al., 2012), which was ascribed to the strengthening of EAWM (**Figure 3**). However, the TEX_{86}-SWT of MZ01 recorded several warming and cooling fluctuations since 6 ka. It represents that the TEX_{86}-SWT of MZ01 is a sensitive

index which not only reflecting the EAWM but also the other impacts such as the Taiwan Warm Current (TWC) and West Kuroshio Branch Current (WKBC) in ECS (see discussion in the next two sections).

Impact of the EAWM and WKBC

Changes in the EAWM over the Holocene have been controversial. The magnetic susceptibility and total organic carbon (TOC) of the Lake Huguang Maar have been used as the indicator of EAWM in the tropics (Yancheva et al., 2007). They show an overall strengthening of EAWM over the Holocene, with episodic weakening during approximately 7–4 ka (Yancheva et al., 2007; **Figure 3A**). Stronger EAWM in the late Holocene has also been supported by marine records in the northern SCS. The vertical and east-west gradient of reconstructed temperatures in the SCS also show that the EAWM became stronger since ∼4 ka (Huang et al., 2011; Steinke et al., 2011). The significant decrease of $U^{K'}_{37}$-SST in coastal areas and the increased gradient between the open sea of the northern SCS have also been proposed to be caused by stronger EAWM in the late Holocene (Kong et al., 2014).

The $U^{K'}_{37}$-SST-trend of MZ01 shows an increase during approximately 7–3 ka and a decrease during 3–0 ka, in good agreement with changes of EAWM in these two periods. It suggests that the long term variability of $U^{K'}_{37}$-SST was controlled by the EAWM in the inner shelf of ECS, comparable to the SCS (Kong et al., 2014, 2017). Though the $U^{K'}_{37}$ is considered a proxy of annual mean SST, some modern investigations suggest the alkenone-producing coccolithophores are more abundant in colder seasons in tropical and sub-tropical seas (Chen et al., 2007). Even if we ignore the seasonality of alkenone production, the larger variability of winter SST would contribute more to the long-term variability of sediment $U^{K'}_{37}$ and thus reflect colder season temperature changes.

The TEX_{86}-SWT-trend of MZ01 exhibits an overall decrease from approximately 6 ka to 4 ka and an increase since ∼4 ka (**Figure 3**). This is in opposite to the trend in the $U^{K'}_{37}$-SST. The discrepancy may lie in the different temperatures that TEX_{86} and $U^{K'}_{37}$ recorded. It has been proposed that the TEX_{86} reflects the bottom water temperature in the ECS (Xing et al., 2015; Yuan et al., 2018), while the $U^{K'}_{37}$ is widely accepted as a SST indicator (Nakanishi et al., 2012; Yuan et al., 2018). Therefore, the opposite changes in these two proxies suggest different controlling mechanisms for temperature change at the surface and bottom of the sea.

To understand this mechanism, it is of prime importance to investigate the modern hydrographic conditions. Modern observed temperature (1955–2012, WOA2013) shows very distinctive seasonal distributions in our studied area (Locarnini et al., 2013; Zweng et al., 2013). The surface temperature is ∼2°C higher than the subsurface (55 m) temperature during summer. It's easy to understand this, as strong stratification dampens the heat convection to deeper waters. In contrast, the subsurface temperature is ∼1°C higher than the surface during fall and winter. And according to the WOA2013 observation data, the mean annual temperature difference between the sea surface and bottom water at MZ01 is around 3–5°C. This phenomenon is quite extraordinary as it's usually thought that the EAWM induced strong mixing that would make the upper layer of the ocean almost homogenous. Nevertheless, the mixing might be weakened by the stratification in the ECS shelf even during cold seasons (Wu, 2015; Xuan et al., 2017). Though the Changjiang River fluxes in winter and fall are not as large as in summer, the plume is driven southwardly by the EAWM and forms a diluted water layer in the ECS. In addition, the TWC and WKBC carry high temperature and salinity water to the ECS shelf and encounter the diluted water (Kako et al., 2016; Wang et al., 2017). The diluted water confronts the warmer and saltier Kuroshio water, dampening the vertical mixing, and heat exchange. As a result, the subsurface water remains warmer when the EAWM causes strong cooling in the diluted surface (Wang and Oey, 2016).

In short, the fluctuations of SST and SWT at MZ01 site are closely associated with the intensity of EAWM and its induced WKBC intrusion. The opposite trends of SST and SWT from approximately 6 ka to 4 ka observed in this study supports this mechanism. The $U^{K'}_{37}$-SST has been increased by weakened EAWM, which may block the intrusions of TWC and WKBC that would decreased the TEX_{86}-SWT. Similarly, stronger EAWM prevailed since 4 ka has promoted the SST decreased and reinforced the TWC and WKBC intrusions, resulting in the TEX_{86}-SWT in the ECS from 4 ka.

Holocene Hydrographic Changes in the ECS

The TEX_{86}-SWT of MZ01 shows several warming-cooling cycles, with episodic peaks at approximately 7.1, 6.0, 2.8, 1.7, and 0.4 ka (**Figure 3**). The HHT spectrum exhibits cyclicity of about 1000–2000 years over the last 8000 years (**Figure 4**). This cyclicity was comparable to the 1500-year quasi-periodicity of the drift-ice record from the north Atlantic (Bond et al., 1997; Bond et al., 2001). Despite some minor mismatch in the ages, the major warmings in the TEX_{86}-SWT show patterns similar to the increase of drift-ice, which were reflected by the hematite-stained grains (HSG) changes in the sediment (**Figure 3A**). The drift-ice indicated large amount of fresh water into the North Atlantic, causing shut down of the AMOC and cold events in the North Atlantic. This process possibly amplified the signal of solar signals and transmitted them globally (Bond et al., 2001). To test the impact of this process in the ECS, we run the hosing experiment as described in the method section. The results show the surface salinity and temperature in the ECS shelf would significantly decrease during Bond's cold events. In contrast, the subsurface (47 m) exhibits much less freshening, particularly in boreal winter (**Figure 2**). This is likely due to the strengthening of the winter monsoon and the fact that the more diluted water of Changjiang River was driven southward. Consequently, the surface salinity dropped greatly in the studied area. While the subsurface water in the ECS shelf was affected by the intrusion of TWC and WKBC, it thus experienced less

freshening. This process would intensify stratification and may have led to the subsurface warming in contrast to the apparent surface cooling.

The sediment grain size of core MD06-3040, which is about 200 km north to the MZ01 on the inner shelf of ECS, was used to study the Changjiang River drainage (Wang et al., 2014; Wang et al., 2020). It was found that the discharge of the Changjiang River has decreased from approximately 6 to 4 ka, then increased by ∼3 ka. The discharge has dropped again by 2.5 ka, with subsequently increased to 1.8 ka, and decreased to 1 ka (**Figure 3B**). The overall pattern of the Changjiang River discharge since 6 ka was in-phase with our TEX_{86}-derived temperature of MZ01. The grain size shows good agreement with the East Asian summer monsoon (EASM) derived from the Dongge Cave stalagmite $\delta^{18}O$ from 6 to 2 ka (Dykoski et al., 2005; **Figure 3B**). After 2 ka, the $\delta^{18}O$ derived EASM intensified, while the grain size indicates the Changjiang discharge decreased (Zhao et al., 2013). This might relate to the asynchronous performance of EASM at different latitudes (An et al., 2000), the location of Western subtropical high (Xu et al., 2019), or the southward migration of ITCZ since 2 ka (Haug et al., 2001).

Further, the variation pattern of the TEX86-derived temperature of MZ01 not only coincides with that of Changjiang River discharge but also shares a similar pattern with the lake level of Chenghai which affected by the summer monsoon precipitation in subtropical East Asia (Xu et al., 2020; **Figure 3B**). The TEX_{86}-SWT of MZ01 and Changjiang River discharge are both characterized by a decreasing trend since 6 ka to a minimum at 4 ka. It implies the EASM has become weak and/or the ITCZ has moved southward during the interval. With the evidence indicated here we argue that the precipitation in the northern region (at the latitude of Chenghai Lake and Changjiang River drainage) has been reduced but might maintained in the south (Dykoski et al., 2005). Reduced precipitation would make the flux of Changjiang Diluted Water (CDW) decreased, that in turn, would make fresh water barrier layer near the coast of the ECS thin, heat convection from the subsurface water increased and thus the TEX_{86}-SWT decreased at site MZ01. The similar migration of ITCZ and weakened EASM with cooling TEX86-derived SWT of MZ01 have happened persistently at ∼2.5 ka, and ∼1 ka (**Figure 3B**).

In contrast, the rising levels of Lake Chenghai between 4–3, 2.5–1.8, and 1–0.4 ka coincide with the increases of Changjiang River discharge and MZ01 TEX_{86}-SWT, suggesting stronger EASM and/or a northern migration of ITCZ (**Figure 3B**). Stronger EASM would lead to more CDW flowing into the ECS and a thicker fresh water barrier layer. In winter, such a thicker barrier layer could dampen heat release of the subsurface water and thus lead to temperature increase. This could be observed from the vertical temperature profile in winter. Surface water has lower salinity and temperature than subsurface shoreward (**Supplementary Figure S1**). But salinity becomes homogenous and surface temperature is higher than subsurface off shore. This feature could be explained by the intrusion of TWC and WKBC on shoreward (Lie and Cho, 2016). Though there is no observational evidence that the TWC and WKBC could reach as shallow as the core MZ01 site, they are speculated here to exert some influence on regional hydrological conditions at millennial scales.

CONCLUSION

The proxies $U^{K'}_{37}$ and TEX_{86} from sediment core MZ01 in the ECS are used to indicate SST and SWT changes over the last 8400-years. After being filtered with the Ensemble Empirical Mode Decomposition (EEMD) of HHT, the fluctuating SST and SWT both have a quasi-periodicity of approximately 1000–2000 years, in accordance with the north Atlantic drift ice activities. This suggests the impact of high latitude forcings on the ECS climate changes. The variability of SST and SWT at centennial and millennial scales reveals some anti-phase since 6 ka. Decrease of SST since approximately 3 ka suggests a cooling effect from intensified Asian winter monsoons and the CCC. This process could also lead to a thicker fresh water barrier layer on the surface, which could apparently dampen heat loss from the bottom water that is evidenced by modern observations. Therefore, the increase of SWT since approximately 4 ka, likely indicates regional hydrographic changes that relate to stronger winter and summer monsoons, as well as possibly stronger WKBC and TWC. The hosing experiment is also lends support to more obvious stratification during the cold period in north Atlantic high latitudes. Finally, our results revealed a close relationship between paleo-temperatures and hydrographic conditions, particularly in the western Pacific marginal seas, and provided a new approach to assess the interaction between regional hydrographic conditions and global climate forcing.

DATA AVAILABILITY STATEMENT

All datasets generated for this study are included in the article/**Supplementary Material**.

AUTHOR CONTRIBUTIONS

M-TC designed the research. H-JP and DK composed the main text and **Supplementary Material**. XL ran the hosting experiment. K-TW was responsible for the CSECM calculation. H-LT, SL, XS, and YY conducted the data analysis.

FUNDING

This study was supported by the research projects MOST 108-2116-M-019-004 and MOST 108-2116-M-019-008-MY2 from the Ministry of Science and Technology, Taiwan.

SUPPLEMENTARY MATERIAL

The Supplementary Material for this article can be found online at: https://www.frontiersin.org/articles/10.3389/feart.2020.00200/full#supplementary-material

REFERENCES

An, Z., Porter, S. C., Kutzbach, J. E., Xihao, W., Suming, W., Xiaodong, L., et al. (2000). Asynchronous Holocene optimum of the East Asian monsoon. *Quatern. Sci. Rev.* 19, 743–762. doi: 10.1016/S0277-3791(99)00031-31

Bian, C., Jiang, W., and Greatbatch, R. J. (2013). An exploratory model study of sediment transport sources and deposits in the Bohai Sea, Yellow Sea, and East China Sea. *J. Geophys. Res. Oceans* 118, 5908–5923. doi: 10.1002/2013JC009116

Bond, G., Kromer, B., Beer, J., Muscheler, R., Evans, M. N., Showers, W., et al. (2001). Persistent solar influence on North Atlantic climate during the holocene. *Science* 294, 2130–2136. doi: 10.1126/science.1065680

Bond, G., Showers, W., Cheseby, M., Lotti, R., Almasi, P., deMenocal, P., et al. (1997). A pervasive millennial-scale cycle in North Atlantic holocene and glacial Climates. *Science* 278, 1257–1266. doi: 10.1126/science.278.5341.1257

Chen, Y.-L. L., Chen, H.-Y., and Chung, C.-W. (2007). Seasonal variability of coccolithophore abundance and assemblage in the northern South China Sea. *Deep Sea Res. II Top. Stud. Oceanogr.* 54, 1617–1633. doi: 10.1016/j.dsr2.2007.05.005

Conte, M. H., Sicre, M.-A., Rühlemann, C., Weber, J. C., Schulte, S., Schulz-Bull, D., et al. (2006). Global temperature calibration of the alkenone unsaturation index (UK′37) in surface waters and comparison with surface sediments. *Geochem. Geophys. Geosyst.* 7:GC001054. doi: 10.1029/2005GC001054

Dykoski, C. A., Edwards, R. L., Cheng, H., Yuan, D., Cai, Y., Zhang, M., et al. (2005). A high-resolution, absolute-dated Holocene and deglacial Asian monsoon record from Dongge Cave, China. *Earth Planet. Sci. Lett.* 233, 71–86. doi: 10.1016/j.epsl.2005.01.036

Haug, G. H., Hughen, K. A., Sigman, D. M., Peterson, L. C., and Röhl, U. (2001). Southward migration of the intertropical convergence zone through the holocene. *Science* 293:1304. doi: 10.1126/science.1059725

Huang, E., Tian, J., and Steinke, S. (2011). Millennial-scale dynamics of the winter cold tongue in the southern South China Sea over the past 26 ka and the East Asian winter monsoon. *Quatern. Res.* 75, 196–204. doi: 10.1016/j.yqres.2010.08.014

Huguet, C., Kim, J.-H., Sinninghe Damsté, J. S., and Schouten, S. (2006). Reconstruction of sea surface temperature variations in the Arabian Sea over the last 23 kyr using organic proxies (TEX86 and $U^{K'}_{37}$). *Paleoceanography* 21:PA3003. doi: 10.1029/2005PA001215

Hung, T.-Y. (2013). *The Application of TEX86 and BIT organic biomarkers to reconstruct climate chagnes in the East China Sea over the past 8000 years*. Keelung: National Taiwan Ocean University.

Jia, G., Zhang, J., Chen, J., Peng, P. A., and Zhang, C. L. (2012). Archaeal tetraether lipids record subsurface water temperature in the South China Sea. *Organ. Geochem.* 50, 68–77. doi: 10.1016/j.orggeochem.2012.07.002

Jian, Z., Wang, P., Saito, Y., Wang, J., Pflaumann, U., Oba, T., et al. (2000). Holocene variability of the Kuroshio Current in the Okinawa Trough, northwestern Pacific Ocean. *Earth Planet. Sci. Lett.* 184, 305–319. doi: 10.1016/S0012-821X(00)00321-326

Kako, S. I, Nakagawa, T., Takayama, K., Hirose, N., and Isobe, A. (2016). Impact of changjiang river discharge on sea surface temperature in the East China Sea. *J. Phys. Oceanogr.* 46, 1735–1750. doi: 10.1175/JPO-D-15-0167.1

Kang, L. K., Lu, H. M., Sung, P. T., Chan, Y. F., Lin, Y. C., Gong, G. C., et al. (2016). The summer distribution of coccolithophores and its relationship to water masses in the East China Sea. *J. Oceanogr.* 72, 883–893. doi: 10.1007/s10872-016-0385-x

Kim, J.-H., van der Meer, J., Schouten, S., Helmke, P., Willmott, V., Sangiorgi, F., et al. (2010). New indices and calibrations derived from the distribution of crenarchaeal isoprenoid tetraether lipids: implications for past sea surface temperature reconstructions. *Geochim. Cosmochim. Acta* 74, 4639–4654. doi: 10.1016/j.gca.2010.05.027

Kong, D., Wei, G., Chen, M.-T., Peng, S., and Liu, Z. (2017). Northern South China Sea SST changes over the last two millennia and possible linkage with solar irradiance. *Quatern. Int.* 459, 29–34. doi: 10.1016/j.quaint.2017.10.001

Kong, D., Zong, Y., Jia, G., Wei, G., Chen, M. T., and Liu, Z. (2014). The development of late Holocene coastal cooling in the northern South China Sea. *Quatern. Int.* 349, 300–307. doi: 10.1016/j.quaint.2013.08.055

Kubota, Y., Kimoto, K., Tada, R., Oda, H., Yokoyama, Y., and Matsuzaki, H. (2010). Variations of East Asian summer monsoon since the last deglaciation based on Mg/Ca and oxygen isotope of planktic foraminifera in the northern East China Sea. *Paleoceanography* 25:PA4205. doi: 10.1029/2009PA001891

Kubota, Y., Tada, R., and Kimoto, K. (2015). Changes in East Asian summer monsoon precipitation during the Holocene deduced from a freshwater flux reconstruction of the Changjiang (Yangtze River) based on the oxygen isotope mass balance in the northern East China Sea. *Clim. Past* 11:265. doi: 10.5194/cp-11-265-2015

Leduc, G., Schneider, R., Kim, J. H., and Lohmann, G. (2010). Holocene and Eemian sea surface temperature trends as revealed by alkenone and Mg/Ca paleothermometry. *Quatern. Sci. Rev.* 29, 989–1004. doi: 10.1016/j.quascirev.2010.01.004

Lee, H.-J., and Chao, S.-Y. (2003). A climatological description of circulation in and around the East China Sea. *Deep Sea Res. II Top. Stud. Oceanogr.* 50, 1065–1084. doi: 10.1016/S0967-0645(03)00010-19

Li, D., Zhao, M., Tian, J., and Li, L. (2013). Comparison and implication of TEX86 and $U^{K'}_{37}$ temperature records over the last 356kyr of ODP Site 1147 from the northern South China Sea. *Palaeogeogr. Palaeoclimatol. Palaeoecol.* 376, 213–223. doi: 10.1016/j.palaeo.2013.02.031

Li, T., Nan, Q., Jiang, B., Sun, R., Zhang, D., and Li, Q. (2009). Formation and evolution of the modern warm current system in the East China Sea and the Yellow Sea since the last deglaciation. *Chinese J. Oceanol. Limnol.* 27, 237–249. doi: 10.1007/s00343-009-9149-9144

Lie, H.-J., and Cho, C.-H. (2016). Seasonal circulation patterns of the Yellow and East China Seas derived from satellite-tracked drifter trajectories and hydrographic observations. *Prog. Oceanogr.* 146, 121–141. doi: 10.1016/j.pocean.2016.06.004

Lin, D.-C., Chen, M.-T., Yamamoto, M., and Yokoyama, Y. (2014). Millennial-scale alkenone sea surface temperature changes in the northern South China Sea during the past 45,000 years (MD972146). *Quatern. Int.* 333, 207–215. doi: 10.1016/j.quaint.2014.03.062

Liu, J. T., Hsu, R. T., Yang, R. J., Wang, Y. P., Wu, H., Du, X., et al. (2018). A comprehensive sediment dynamics study of a major mud belt system on the inner shelf along an energetic coast. *Sci. Rep.* 8:4229. doi: 10.1038/s41598-018-22696-w

Liu, S., Shi, X., Liu, Y., Qiao, S., Yang, G., Fang, X., et al. (2010). Records of the East Asian winter monsoon from the mud area on the inner shelf of the East China Sea since the mid-Holocene. *Chinese Sci. Bull.* 55, 2306–2314. doi: 10.1007/s11434-010-3215-3213

Locarnini, R. A., Mishonov, A. V., Antonov, J. I., Boyer, T. P., Garcia, H. E., Baranova, O. K., et al. (2013). *World ocean atlas 2013 Temperature*. Silver Spring, MA: NOAA.

Nakanishi, T., Yamamoto, M., Tada, R., and Oda, H. (2012). Centennial-scale winter monsoon variability in the northern East China Sea during the Holocene. *J. Quatern. Sci.* 27, 956–963. doi: 10.1002/jqs.2589

PAGES Ocean 2k Working Group (2012). "Synthesis of marine sediment-derived SST records for the past 2 millennia: first-order results from the PAGES/Ocean2k project," in *Proceedings of the AGU Fall Meeting, PP11F-07* (Washington, DC: American Geophysical Union).

Popp, B. N., Prahl, F. G., Wallsgrove, R. J., and Tanimoto, J. (2006). Seasonal patterns of alkenone production in the subtropical oligotrophic North Pacific. *Paleoceanography* 21, 1–15. doi: 10.1029/2005PA001165

Rodrigues, T., Grimalt, J. O., Abrantes, F. G., Flores, J. A., and Lebreiro, S. M. (2009). Holocene interdependences of changes in sea surface temperature, productivity, and fluvial inputs in the Iberian continental shelf (Tagus mud patch). *Geochem. Geophys. Geosyst.* 10:Q07U06. doi: 10.1029/2008GC002367

Sachs, J. P. (2007). Cooling of Northwest Atlantic slope waters during the Holocene. *Geophys. Res. Lett.* 34:L03609. doi: 10.1029/2006GL028495

Steinke, S., Glatz, C., Mohtadi, M., Groeneveld, J., Li, Q., and Jian, Z. (2011). Past dynamics of the East Asian monsoon: no inverse behaviour between the summer and winter monsoon during the Holocene. *Glob. Planet. Change* 78, 170–177. doi: 10.1016/j.gloplacha.2011.06.006

Stouffer, R. J., Yin, J., Gregory, J. M., Dixon, K. W., Spelman, M. J., Hurlin, W., et al. (2006). Investigating the causes of the response of the thermohaline circulation to past and future climate changes. *J. Clim.* 19, 1365–1387. doi: 10.1175/JCLI3689.1

Svendsen, L., Kvamstø, N. G., and Keenlyside, N. (2014). Weakening AMOC connects Equatorial Atlantic and Pacific interannual variability. *Clim. Dyn.* 43, 2931–2941. doi: 10.1007/s00382-013-1904-1908

Tierney, J. E., and Tingley, M. P. (2014). A Bayesian, spatially-varying calibration model for the TEX86 proxy. *Geochim. Cosmochim. Acta* 127, 83–106. doi: 10.1016/j.gca.2013.11.026

Tierney, J. E., and Tingley, M. P. (2015). A TEX86 surface sediment database and extended Bayesian calibration. *Sci. Data* 2, 1–10. doi: 10.1038/sdata.2015.29

Tsai, H. L. (2013). *The Application of Alkenone Unsaturation Organic Biomarkers to Reconstruct Sea Surface Temperature and Climate Changes in the East China Sea over the Past 8000 years*. Keelung: National Taiwan Ocean University.

van Oldenborgh, G. J., te Raa, L. A., Dijkstra, H. A., and Philip, S. Y. (2009). Frequency- or amplitude-dependent effects of the Atlantic meridional overturning on the tropical Pacific Ocean. *Ocean Sci.* 5, 293–301. doi: 10.5194/os-5-293-2009

Wang, B., Hirose, N., Yuan, D., Moon, J.-H., and Pan, X. (2017). Effects of tides on the cross-isobath movement of the low-salinity plume in the western Yellow and East China Seas in winter. *Continent. Shelf Res.* 143, 228–239. doi: 10.1016/j.csr.2016.06.011

Wang, J., and Oey, L. Y. (2016). Seasonal exchanges of the kuroshio and shelf waters and their impacts on the shelf currents of the East China Sea. *J. Phys. Oceanogr.* 46, 1615–1632. doi: 10.1175/JPO-D-15-0183.1

Wang, K., Tada, R., Zheng, H., Irino, T., Zhou, B., and Saito, K. (2020). Provenance changes in fine detrital quartz in the inner shelf sediments of the East China Sea associated with shifts in the East Asian summer monsoon front during the last 6 kyrs. *Prog. Earth Planet. Sci.* 7:5. doi: 10.1186/s40645-019-0319-315

Wang, K., Zheng, H., Tada, R., Irino, T., Zheng, Y., Saito, K., et al. (2014). Millennial-scale East Asian Summer Monsoon variability recorded in grain size and provenance of mud belt sediments on the inner shelf of the East China Sea during mid-to late Holocene. *Quatern. Int.* 349, 79–89. doi: 10.1016/j.quaint.2014.09.014

Wei, Y., Wang, J., Liu, J., Dong, L., Li, L., Wang, H., et al. (2011). Spatial variations in archaeal lipids of surface water and core-top sediments in the South China Sea and their implications for paleoclimate studies. *Appl. Environ. Microbiol.* 77:7479. doi: 10.1128/AEM.00580-511

Wu, H. (2015). Cross-shelf penetrating fronts: a response of buoyant coastal water to ambient pycnocline undulation. *J. Geophys. Res. Oceans* 120, 5101–5119. doi: 10.1002/2014JC010686

Xing, L., Sachs, J. P., Gao, W., Tao, S., Zhao, X., Li, L., et al. (2015). TEX86 paleothermometer as an indication of bottom water temperature in the Yellow Sea. *Organ. Geochem.* 86, 19–31. doi: 10.1016/j.orggeochem.2015.05.007

Xu, H., Goldsmith, Y., Lan, J., Tan, L., Wang, X., Zhou, X., et al. (2020). Juxtaposition of western pacific subtropical high on asian summer monsoon shapes subtropical east asian precipitation. *Geophys. Res. Lett.* 47:e2019GL084705. doi: 10.1029/2019GL084705

Xu, H., Song, Y., Goldsmith, Y., and Lang, Y. (2019). Meridional ITCZ shifts modulate tropical/subtropical Asian monsoon rainfall. *Sci. Bull.* 64, 1737–1739. doi: 10.1016/j.scib.2019.09.025

Xuan, J., Huang, D., Pohlmann, T., Su, J., Mayer, B., Ding, R., et al. (2017). Synoptic fluctuation of the Taiwan Warm Current in winter on the East China Sea shelf. *Ocean Sci.* 13:55332710.

Yancheva, G., Nowaczyk, N. R., Mingram, J., Dulski, P., Schettler, G., Negendank, J. F. W., et al. (2007). Influence of the intertropical convergence zone on the East Asian monsoon. *Nature* 445, 74–77. doi: 10.1038/nature05431

Yang, S., Bi, L., Li, C., Wang, Z., and Dou, Y. (2016). Major sinks of the Changjiang (Yangtze River)-derived sediments in the East China Sea during the late Quaternary. *Geol. Soc.* 429, 137–152. doi: 10.1144/sp429.6

Yi, L., Chen, S., Ortiz, J. D., Chen, G., Peng, J., Liu, F., et al. (2015). 1500-year cycle dominated Holocene dynamics of the Yellow River delta. China. *Holocene* 26, 222–234. doi: 10.1177/0959683615596834

Yuan, Z., Xiao, X., Wang, F., Xing, L., Wang, Z., Zhang, H., et al. (2018). Spatiotemporal temperature variations in the East China Sea shelf during the Holocene in response to surface circulation evolution. *Quatern. Int.* 482, 46–55. doi: 10.1016/j.quaint.2018.04.025

Zhang, J., Bai, Y., Xu, S., Lei, F., and Jia, G. (2013). Alkenone and tetraether lipids reflect different seasonal seawater temperatures in the coastal northern South China Sea. *Organ. Geochem.* 58, 115–120. doi: 10.1016/j.orggeochem.2013.02.012

Zhang, J., Jia, G., Guo, W., Wang, X., and Lei, F. (2017). Isoprenoid tetraether lipids in suspended particulate matter from the East China Sea and implication for sedimentary records. *Organ. Geochem.* 114, 81–90. doi: 10.1016/j.orggeochem.2017.09.006

Zhao, C., Chang, Y.-P., Chen, M.-T., and Liu, Z. (2013). Possible reverse trend in Asian summer monsoon strength during the late Holocene. *J. Asian Earth Sci.* 69, 102–112. doi: 10.1016/j.jseaes.2012.09.028

Zhao, M., Ding, L., Xing, L., Qiao, S., and Yang, Z. (2014). Major mid-late Holocene cooling in the East China Sea revealed by an alkenone sea surface temperature record. *J. Ocean Univ. China* 13, 935–940. doi: 10.1007/s11802-014-2641-2642

Zweng, M. M., Reagan, J. R., Antonov, J. I., Locarnini, R. A., Mishonov, A. V., Boyer, T. P., et al. (2013). *World Ocean Atlas 2013 Salinity*. Silver Spring, MA: NOAA.

Conflict of Interest: The authors declare that the research was conducted in the absence of any commercial or financial relationships that could be construed as a potential conflict of interest.

Copyright © 2020 Pan, Chen, Kong, Lin, Wong, Tsai, Liu, Shi and Yokoyama. This is an open-access article distributed under the terms of the Creative Commons Attribution License (CC BY). The use, distribution or reproduction in other forums is permitted, provided the original author(s) and the copyright owner(s) are credited and that the original publication in this journal is cited, in accordance with accepted academic practice. No use, distribution or reproduction is permitted which does not comply with these terms.